Gluon distributions in nuclei probed at energies available at the CERN Large Hadron Collider

Adeola Adeluyi and Carlos A. Bertulani
Department of Physics & Astronomy, Texas A&M University–Commerce, Commerce, TX 75428, USA
(Received 27 May 2011; revised manuscript received 24 July 2011; published 29 August 2011)

Using updated gluon distributions from global fits to data, we investigate the sensitivity of direct photoproduction of heavy quarks and exclusive production of vector mesons to varying strength of gluon modifications. Implications of using these processes for constraining nuclear gluon distributions are discussed.

DOI: 10.1103/PhysRevC.84.024916 PACS number(s): 24.85.+p, 25.30.Dh, 25.75.−q

I. INTRODUCTION

Ultraperipheral relativistic heavy ion collisions can explore several aspects of particle and nuclear physics and have been extensively discussed in the literature (for a small sample of references see, e.g., [1–12]). In this article, we investigate the sensitivity of direct photoproduction of heavy quarks and exclusive production of vector mesons to different gluon distribution functions. This idea, originally proposed in Ref. [7], can be used to constrain the possible distribution functions from data on production of heavy quarks and of vector mesons. Here we report on the study of certain distribution functions not considered so far.

A key ingredient of our calculations, the photon flux in ultraperipheral collisions, can be evaluated by the equivalent photon (Weizsäcker-Williams) method [1]. Improvements to the method have been documented in several publications [2–4]. For a given impact parameter **b**, the flux of virtual photons with photon energy k is $d^3N_\gamma(k,\mathbf{b})/dkd^2b$, depending strongly on the Lorentz factor γ. At the Large Hadron Collider (LHC) at CERN the Lorentz γ_L factor in the laboratory frame is 7455 for $p-p$ and 2930 for Pb-Pb collisions. The photon flux also depends strongly on the adiabaticity parameter $\zeta = kb/\gamma$ [2–4]:

$$\frac{d^3N_\gamma(k,\mathbf{b})}{dkd^2b} = \frac{Z^2\alpha\zeta^2}{\pi^2kb^2}\left[K_1^2(\zeta)+\frac{1}{\gamma_L^2}K_0^2(\zeta)\right]. \qquad (1)$$

Due to the modified Bessel functions $K_0(\zeta)$ and $K_1(\zeta)$, the photon flux possesses the asymptotic property of an exponential dropoff at $\zeta > 1$, above a cutoff energy determined essentially by the size of the nucleus, $E_{\rm cutoff} \sim \gamma$ MeV $/b$ (fm). The relationship between the Lorentz contraction factor associated with the relative velocity between the colliding nuclei, and the collider energy per nucleon, E/A, in GeV, is given by $\gamma = 2\gamma_L^2 - 1 \approx 2(1.0735E/A)^2$.

Integrating $d^3N_\gamma(k,\mathbf{b})/dkd^2b$ over impact parameters with the constraint of no hadronic interactions yields the total photon flux $dN_\gamma(k)/dk$. An analytic expression for this total flux, strongly dependent on the reduced adiabaticity parameter $\zeta_R^{AA} = 2kR_A/\gamma$ for AA collisions, or $\zeta_R^{pA} = k(R_p+R_A)/\gamma$ for pA collisions, is derivable in the approximation whereby Eq. (1) is integrated over impact parameters larger than the sum of the radii of the participants. While this is a good approximation, a relatively better estimate of the total flux is obtained by taking the average over the target surface [5,11],

$$\frac{dN_\gamma(k)}{dk} = 2\pi\int_{2R_A}^{\infty} db\, b\int_0^R \frac{dr\, r}{\pi R_A^2}\int_0^{2\pi} d\phi \times \frac{d^3N_\gamma(k,b+r\cos\phi)}{dkd^2b}\,. \qquad (2)$$

Although both the analytic expression and Eq. (2), evaluated numerically, have been utilized in the present study, we report only results using the numerical flux. The differences between the results from analytic and numerical fluxes are generally of the order of 10%–15%. With the knowledge of the photon flux, any generic total photoproduction cross section can be factorized into the product of a photonuclear cross section $\sigma_X^\gamma(k)$ and the photon flux, dN_γ/dk, $\sigma_X = \int dk(dN_\gamma/dk)\sigma_X^\gamma(k)$.

The photonuclear processes described in the present work are dependent on gluon distributions in nuclei. This dependence influences the structural characteristics of these processes, especially in the case of the exclusive photoproduction of vector mesons, in which the gluon distribution enters quadratically. It is a rather well-known fact that the distributions of partons (i.e., quarks and gluons) in nuclei are quite different from the distributions in free nucleons, due to the complex, many-body effects in the nuclear medium. This is expected to manifest in experimental observables such as the cross section and rapidity distributions.

II. NUCLEAR PARTON DISTRIBUTIONS

Nuclear parton distribution functions, $F_a^A(\mathbf{r},x,Q^2)$, are often for technical convenience expressed as a convolution of "nuclear modifications" $R_a^A(\mathbf{r},x,Q^2)$ and free nucleon parton distribution functions $f_a(x,Q^2)$. Here the subscript a denotes a parton species and the superscript A denotes a particular nucleus. The variables are the position vector **r**, parton momentum fraction x (Bjorken-x), and a hard scale (factorization scale) Q^2. However, since limited availability of data does not permit a determination of the spatial dependence, current nuclear parton distributions from global fits are functions of x and Q^2 only. The nuclear effects encoded in the nuclear modifications $R_a^A(x,Q^2)$ can be categorized based on different intervals in x. At small values of x ($x \lesssim 0.04$), we have the phenomenon generally referred to

as shadowing. This is a depletion, in the sense that in this interval, the nuclear parton distributions are smaller compared to the corresponding distributions in free nucleons, i.e., $R_a^A < 1$. Antishadowing, which is an enhancement ($R_a^A > 1$), occurs in the range $0.04 \lesssim x \lesssim 0.3$. Another depletion, the classic EMC effect [13], is present in the interval $0.3 \lesssim x \lesssim 0.8$; while for $x > 0.8$, the Fermi motion region, we have another enhancement. It is important to note that although both shadowing and the EMC effect (antishadowing and Fermi motion) correspond to depletion (enhancement), the physical principles and mechanisms governing these phenomena are quite different. Further details can be found in [14–17].

The determination of gluon distributions in both nucleons and nuclei is a highly nontrivial task. In the usual determination of parton distributions from global fits to data, a preponderance of the experimental data is from deeply inelastic scattering (DIS) and Drell-Yan (DY) processes. Since gluons are electrically neutral, their distributions cannot be directly extracted from DIS; they are inferred from sum rules and the Q^2 evolution of sea quark distributions. The situation is even worse in the nuclear case: the available data are much less than for nucleons, and there is the added complication of a mass dependence. It is therefore not unusual for nuclear gluon distributions from different global fits to differ significantly, especially in the magnitude of the various nuclear effects (shadowing, antishadowing, etc.). This is especially obvious at low Q^2 (i.e., around their initial starting scales) since evolution to high Q^2 tends to lessen the differences. Earlier global analyses [18–21] relied heavily on fixed-target nuclear deep-inelastic scattering (DIS) and Drell-Yan (DY) lepton-pair production, with the attendant low precision and weak constraints on nuclear gluon distributions. The use of an extended data set, incorporating data on inclusive hadron production in deuteron-gold collisions, has been pioneered in [22,23], with better constraints on gluon modifications. We should also mention the approach in [24] that utilizes the Gribov picture of shadowing. Despite all of these advances the nuclear gluon distribution is still the least constrained aspect of global fits to nuclear parton distributions, as large uncertainties still persist at both small and large x.

Four recent gluon distributions are utilized in the present study. For the nucleon gluon distributions we use the Martin-Stirling-Thorne-Watts (MSTW08) parton distributions [25]. In the nuclear case we use three nuclear modification sets. Two sets are by Eskola, Paukunnen, and Salgado, namely, EPS08 and EPS09 [22,23]. The third is the Hirai-Kumano-Nagai (HKN07) distributions [21]. The gluon distributions from MSTW08 serve two purposes: as the free nucleon distributions used in conjunction with nuclear modifications, and also as a "special" nuclear gluon distribution in the absence of nuclear effects. The latter usage is particularly useful for highlighting the influence of the various nuclear effects on observables. Our calculations are to leading order (LO); thus all distributions are evaluated at this order.

These four gluon distributions have different characteristics due to the different strengths of their nuclear modifications. As already stated, one can view the MSTW08 gluon distributions as nuclear gluon distributions in the limit of zero nuclear effects ($R_a^A = 1$). In Fig. 1 we show the nuclear modifications from EPS08, EPS09, and HKN07 at the factorization scale $Q^2 = M_{J/\Psi}^2$, appropriate for the elastic photoproduction of the J/Ψ meson. At this scale, HKN07 has a rather weak gluon shadowing that extends well into the antishadowing region, no antishadowing and gluon EMC effect, and an early onset of Fermi motion. EPS09 exhibits a moderately strong shadowing, and appreciable antishadowing and EMC effect, with quite a strong Fermi motion. Nuclear modifications are strongest in EPS08: an especially strong shadowing, and substantial antishadowing, EMC, and Fermi motion. Thus in terms of shadowing we have a progression from zero effects to weak effects, to moderate (intermediate) effects, then to strong effects as one progresses from MSTW08 to EPS08. We have not included uncertainties from gluon distributions in this study. Further discussions of uncertainties in nuclear parton distributions can be found in [23].

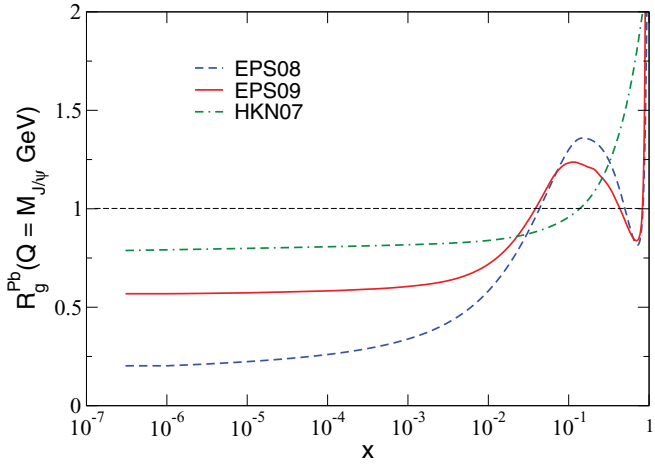

FIG. 1. (Color online) Nuclear gluon modifications in Pb, $R_g^{Pb}(x, Q^2 = M_{J/\Psi}^2)$, from EPS08 (dashed line), EPS09 (solid line), and HKN07 (dash-dotted line), respectively.

From the point of view of a Fock space decomposition, photon interactions with hadrons and nuclei can be direct or resolved. In direct interactions the photon behaves as a point-like particle ("bare photon") while in resolved interactions the photon fluctuates into a quark-antiquark state or an even more complex partonic state. In the present study we will focus attention only on the direct photon contribution. The contribution of resolved photon processes in ultraperipheral heavy-ion collisions is treated in detail in Ref. [8].

III. DIRECT PHOTOPRODUCTION OF HEAVY QUARKS

Photon-gluon fusion leading to the production of a heavy quark pair is the dominant subprocess when high-energy photons are incident on a nucleus. Due to the high energies involved, perturbative QCD is applicable, and the cross section can be expressed as a convolution of the partonic cross section for the subprocess $\gamma g \to q\bar{q}$ and the nuclear gluon

distribution:

$$\sigma^{\gamma A\to q\bar{q}X}(W_{\gamma A}) = \int_{x_{\min}}^{1} dx\, \sigma^{\gamma g\to q\bar{q}}(W_{\gamma g})\, G_A(x, Q^2), \quad (3)$$

with x the momentum fraction carried by the gluon, and $x_{\min} = 4m_q^2/W_{\gamma A}^2$. Here m_q is the mass of the heavy quark (charm or bottom), $W_{\gamma A}$ ($W_{\gamma g}$) denotes the center-of-mass energy of the photon-nucleus (photon-gluon) system, and $G_A(x, Q^2)$ is the nuclear gluon distribution. The pQCD factorization scale Q is quite arbitrary; the cross section is thus scale dependent. In the present study we use two different scales in order to assess the magnitude of scale dependency: a dynamic scale $Q^2 = W_{\gamma g}^2 = \hat{s}$ as in [26], and a static scale $Q^2 = 4m_c^2(m_b^2)$ for charm (bottom), respectively, as in [8]. We take $m_c = 1.4$ GeV and $m_b = 4.75$ GeV for consistency with the MSTW08 parton distributions.

The cross section for the photon-gluon fusion leading to quark pair production is [26–28]

$$\sigma^{\gamma g\to q\bar{q}}(W_{\gamma g}) = \frac{2\pi\,\alpha_{\rm em}\,\alpha_s(Q^2)\,e_q^2}{W_{\gamma g}^2}\left[\left(1+\beta-\frac{1}{2}\beta^2\right)\times \ln\left(\frac{1+\sqrt{1-\beta}}{1-\sqrt{1-\beta}}\right) - (1+\beta)\sqrt{1-\beta}\right], \quad (4)$$

with e_q the electric charge of the quark, $\alpha_{\rm em}$ the electromagnetic coupling constant, and $\beta = 4m_q^2/W_{\gamma g}^2$. The strong coupling constant $\alpha_s(Q^2)$, needed for the calculation, is evaluated to one loop at the scale Q^2 using the evolution code contained in the MSTW08 package. The total photoproduction cross section $\sigma(A[\gamma]A \to Aq\bar{q}X)$ is obtained by convoluting the equivalent photon flux $dN_\gamma(k)/dk$ with $\sigma^{\gamma A\to q\bar{q}X}(k)$:

$$\sigma(A[\gamma]A \to Aq\bar{q}X) = \int dk\, \frac{dN_\gamma(k)}{dk}\,\sigma^{\gamma A\to q\bar{q}X}(k). \quad (5)$$

The final-state $q\bar{q}$ rapidity is dependent on the photon energy k and the gluon momentum fraction x: $x = (W_{\gamma g}/W_{\gamma A})e^y$. Thus changing the variable from k to y and differentiating ($d\sigma/dy = kd\sigma/dk$), the differential cross section with respect to rapidity is thus $d\sigma^{\gamma A\to q\bar{q}X}/dy = [kdN_\gamma(k)/dk]\sigma^{\gamma A\to q\bar{q}X}(k)$.

Both the total cross section and the rapidity distribution involve the product of the photon flux and the photonuclear cross section. The flux decreases exponentially with increasing photon energy k while the cross section, due to its dependence on $x_{\min}$, increases with k since $x_{\min}$ is inversely related to k. This interplay not only decisively influences the magnitude of the total cross section and rapidity distributions, but also the relative contributions of the various x-dependent nuclear modifications of the gluon distribution in $G_A(x, Q^2)$. For instance, gluon shadowing is of less importance in photoproduction of bottom quarks compared to charm quarks. This is due to the fact that the advent of shadowing contribution in $b\bar{b}$ production occurs at a larger photon energy where the flux is more suppressed than in $c\bar{c}$ photoproduction, where the onset occurs at a lower photon energy, and thus with a larger usable photon flux availability.

IV. ELASTIC PHOTOPRODUCTION OF VECTOR MESONS

The differential cross section for the elastic photoproduction of a vector meson V on a nucleus A in the exclusive process $A[\gamma]A \to AAV$ can be written as $d\sigma^{\gamma A\to VA}/dt = d\sigma^{\gamma A\to VA}/dt|_{t=0}|F(t)|^2$, where $d\sigma^{\gamma A\to VA}/dt|_{t=0}$ is the forward-scattering amplitude and $F(t)$ is the nuclear form factor. The dynamical information is encoded in the forward-scattering amplitude while the momentum transfer of the elastic scattering is determined by the form factor, which is dependent on the spatial attributes of the target nucleus.

Diverse mechanisms have been employed in the evaluation of the dynamical content of the forward-scattering amplitude for heavy mesons. In this study we use the simple amplitude calculated from leading-order two-gluon exchange in perturbative QCD [29,30] and corrected for other relevant effects (such as relativistic corrections, inclusion of the real part of the scattering amplitude, next-to-leading-order NLO effects, etc.; see, for instance, [31,32]) through a phenomenological multiplicative correction factor ζ_V. For elastic photoproduction on protons, the corrected LO scattering amplitude can be written as

$$\left.\frac{d\sigma^{\gamma p\to Vp}}{dt}\right|_{t=0} = \zeta_V\left(\frac{16\pi^3\alpha_s^2\,\Gamma_{ee}}{3\alpha M_V^5}\right)[xg_p(x, Q^2)]^2. \quad (6)$$

Here, M_V is the mass of the vector meson [J/Ψ and $\Upsilon(1s)$ in the present study], $x = M_V^2/W_{\gamma p}^2$ is the fraction of the nucleon momentum carried by the gluons, and $g_p(x, Q^2)$ is the gluon distribution in a proton, evaluated at a momentum transfer $Q^2 = (M_V/2)^2$. Equation (6) is easily generalized to the nuclear case:

$$\left.\frac{d\sigma^{\gamma A\to VA}}{dt}\right|_{t=0} = \zeta_V\left(\frac{16\pi^3\alpha_s^2\,\Gamma_{ee}}{3\alpha M_V^5}\right)[xG_A(x, Q^2)]^2, \quad (7)$$

where $G_A(x, Q^2) = g_p(x, Q^2) \times R_g^A(x, Q^2)$ is the nuclear gluon distribution and $R_g^A(x, Q^2)$ is the gluon modification.

The correction factor ζ_V is estimated by constraining the calculated cross sections for elastic vector mesons photoproduction on protons, $\sigma^{\gamma p\to Vp}(W_{\gamma p})$, to reasonably reproduce the photoproduction data from HERA: Ref. [33] for J/Ψ and Refs. [33–35] for $\Upsilon(1s)$. $\sigma^{\gamma p\to Vp}$ is obtained through $\sigma^{\gamma p\to Vp} = (1/b)d\sigma^{\gamma p\to Vp}/dt|_{t=0}$ with slope parameter b. Using $b = 4.5$ GeV^{-2}, we have $\zeta_{J/\Psi} = 1/3.5$ and $\zeta_{\Upsilon(1s)} = 1.0$, and the results are displayed in Fig. 2. $\zeta_{\Upsilon(1s)} = 1.0$ for the elastic photoproduction of Υ underestimates older HERA data [33,34] but seems to be adequate for the newer analysis in [35]. This could indicate the smallness of higher-order effects and other corrections, whereas they are of major importance in J/Ψ production.

In contrast to photoproduction of heavy quarks, the quadratic dependence of the differential cross section on the gluon distribution has the significant implication of making exclusive vector meson production a very sensitive probe of nuclear gluon modifications. This is apparent from Fig. 3, where the forward-scattering amplitude for J/Ψ production in Pb-Pb collisions at LHC energy is plotted as a function of x for the four gluon distributions under consideration. The different characteristics displayed in Fig. 1 are clearly manifested.

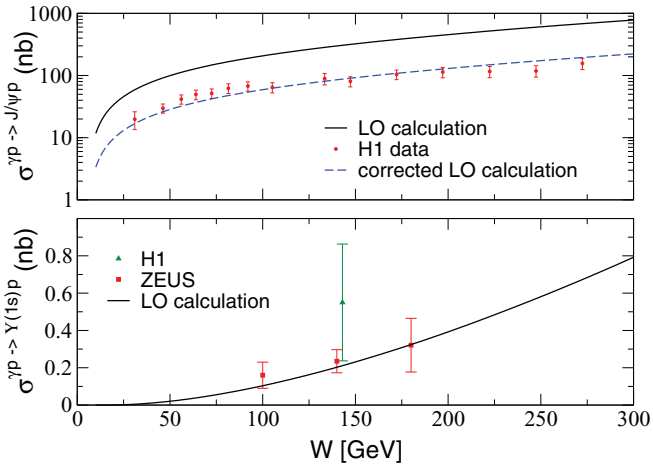

FIG. 2. (Color online) Cross section for photoproduction of J/Ψ (Υ) as a function of energy $W_{\gamma p}$. In the upper panel the solid line is the LO result while the dashed line is the corrected LO result using $\zeta_{J/\Psi} = 1/3.5$, with data from [33]. In the lower panel data are taken from [33,35] and the solid line depicts the LO result.

The nuclear form factor $F(t)$ is given by the Fourier transform of the nuclear density distribution: $F(t) = \int d^3r\, \rho(r)\, e^{i\mathbf{q}\cdot\mathbf{r}}$, where q is the momentum transferred. For a heavy nucleus it is customary to model the density distribution as a Woods-Saxon distribution with parameters from electron scattering, $\rho(r) = \rho_0/[1 + e^{[(r-R_A)/d]}]$, with central density ρ_0, radius R_A and skin depth d. For ^{208}Pb in use at the LHC, $\rho_0 = 0.16/\text{fm}^3$, $R_A = 1.2A^{1/3}$ fm, and $d = 0.549$ fm [36]. Since the Fourier transform of a Woods-Saxon density distribution does not admit of an analytic form, we employed the commonly used modified hard sphere (a convolution of a hard sphere with a Yukawa term) [5,6,37] to approximate $\rho(r)$ in $F(t)$:

$$F(q = \sqrt{|t|}) = \frac{4\pi\rho_0}{Aq^3}[\sin(qR_A) - qR_A\cos(qR_A)]\left[\frac{1}{1+a^2q^2}\right]. \quad (8)$$

The range of the Yukawa term a is 0.7 fm, and the form factor is a simple product of the Fourier transforms of the hard sphere and the Yukawa term.

The photonuclear cross section is thus given by

$$\sigma^{\gamma A\to VA}(k) = \left.\frac{d\sigma^{\gamma A\to VA}}{dt}\right|_{t=0}\int_{t_{\min}(k)}^{\infty} dt|F(t)|^2. \quad (9)$$

Here $t_{\min}(k) = (M_v^2/4k\gamma_L)^2$, as is appropriate for narrow resonances [38]. The total cross section is a convolution of the photonuclear cross section and the photon flux:

$$\sigma^{A[\gamma]A\to AAV} = \int dk\frac{dN_\gamma(k)}{dk}\sigma^{\gamma A\to VA}(k) = \int dk\frac{dN_\gamma(k)}{dk}\int_{t_{\min}(k)}^{\infty} dt\left.\frac{d\sigma^{\gamma A\to VA}}{dt}\right|_{t=0}|F(t)|^2. \quad (10)$$

It is often of practical interest to represent the cross section in terms of the rapidity of the vector meson. The photon energy k is related to the rapidity y by $k = (M_V/2)\exp(y)$. Using this relationship, the differential cross section with respect to rapidity is given by $d\sigma^{\gamma A\to VA}/dy = [kdN_\gamma(k)/dk]\sigma^{\gamma A\to VA}(k)$. Thus with a knowledge of the photon flux the differential cross section $d\sigma/dy$ is a direct measure of the vector meson photoproduction cross section for a given photon energy.

We now discuss the results of our calculations for both the inclusive photoproduction of heavy quarks ($c\bar{c}$ and $b\bar{b}$) and the exclusive production of vector mesons [J/Ψ and $\Upsilon(1s)$]. For the cross sections for heavy quarks we present results for the two scales employed: a dynamic scale $Q^2 = \hat{s}$ and a static scale $Q^2 = 4m_c^2$ ($Q^2 = m_b^2$) for charm (bottom), while for the vector mesons we present both the LO and corrected LO results. In the case of rapidity distributions we show only the result for the dynamic scale for heavy quarks, and the corrected LO for the vector mesons. Since we deal with symmetric Pb-Pb collisions, both nuclei can serve as source and/or target and the total rapidity distribution is the sum of both, and symmetric about $y = 0$.

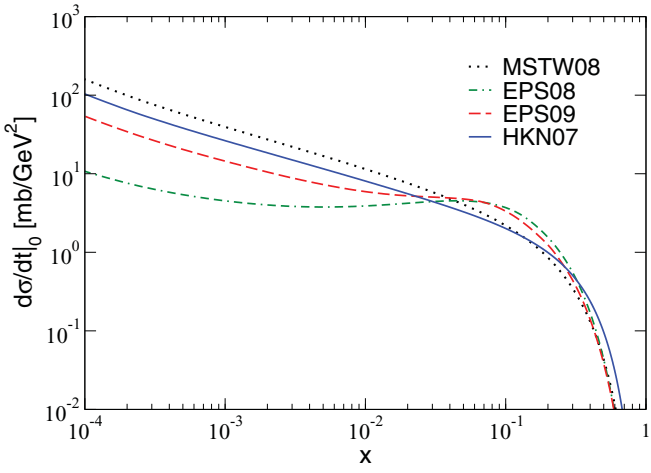

FIG. 3. (Color online) Forward-scattering amplitude for elastic photoproduction of J/Ψ in Pb-Pb collisions as a function of momentum fraction x for four different gluon distributions. Dotted line depicts result using the MSTW08 gluon distribution (no nuclear modifications). Dashed, dot-dashed, and solid lines are results from nuclear-modified gluon distributions from EPS09, EPS08, and HKN07 parton distributions, respectively.

V. GLUON MODIFICATIONS IN PHOTOPRODUCTION OF HEAVY QUARKS

The sensitivity of heavy quark photoproduction to nuclear gluon modifications is more transparent in rapidity distributions than in total cross sections. In Fig. 4 we show the rapidity distributions for $c\bar{c}$ production in ultraperipheral Pb-Pb collisions at the LHC, employing the four gluon distributions described earlier. The upper panel depicts the distributions with the incident photon coming from the right, while the lower panel shows the distributions with the incident photons from the left. The total, which is the sum of both panels, is displayed in Fig. 5.

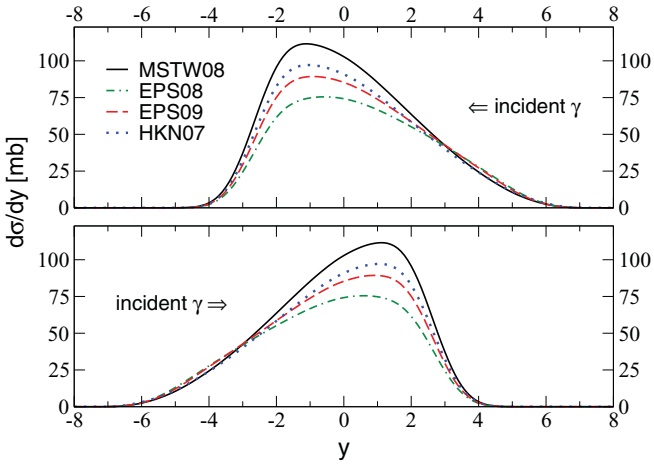

FIG. 4. (Color online) Rapidity distributions of $c\bar{c}$ photoproduction in Pb-Pb collisions at the LHC for photons incident from the right (upper panel) and from the left (lower panel). Solid line depicts the result using the MSTW08 gluon distribution (no nuclear modifications). Dashed, dot-dashed, and dotted lines are results from nuclear-modified gluon distributions from EPS09, EPS08, and HKN07 parton distributions, respectively.

As mentioned earlier, the value of $x_{\min}(k)$ determines the nuclear effects contributing to the photonuclear cross section $\sigma^{\gamma A\to q\bar{q}X}(k)$. Since the rapidity distribution $d\sigma/dy$ is directly proportional to this cross section, it is rather straightforward to elucidate the features of the rapidity distribution based on the relative contributions of the relevant nuclear effects. Figure 1 is thus quite helpful in understanding the characteristics of the distributions displayed in Fig. 4 and, by extension, Fig. 5.

Let us start from midrapidity ($y = 0$) and move toward higher positive values of y. In the upper panel of Fig. 4 (photons from right), the contribution from shadowing becomes progressively smaller, such that at around $y = 3$ shadowing is negligible and antishadowing becomes the dominant contributor. At around $y = 6$ antishadowing peters out, and the distributions are subject only to EMC/Fermi motion effects. On the other hand, for the lower panel in Fig. 4 (photons from left), shadowing becomes progressively stronger and more dominant for increasing y. The effect of shadowing in this region is mitigated by the rather strong suppression of the photon flux at large k; the distributions thus rapidly die out with increasing positive y. The opposite trend is observed for increasingly negative y values starting from midrapidity. Here, for photons incident from the right (upper panel), increasing negative values of y implies increasing shadowing and flux suppression. For photons incident from the left (lower panel), the transition is from shadowing to EMC/Fermi motion effects.

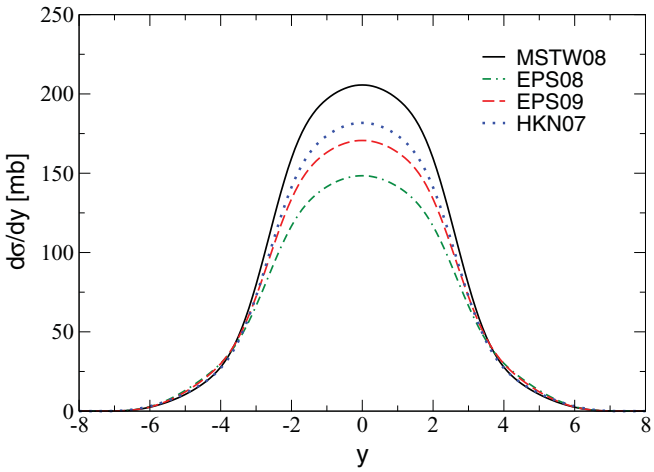

FIG. 5. (Color online) Total rapidity distributions of the photoproduction of $c\bar{c}$ in Pb-Pb collisions at the LHC. Solid line depicts the result using the MSTW08 gluon distribution (no nuclear modifications). Dashed, dot-dashed, and dotted lines are results from nuclear-modified gluon distributions from EPS09, EPS08, and HKN07 parton distributions, respectively.

We now consider the characteristics of the total rapidity distributions due to the amalgamation of the contrasting tendencies exhibited in the upper and lower panels of Fig. 4. Shadowing is the dominant nuclear effect for $-3 < y < 3$, and the rapidity distributions in this region reproduce the observed trend of gluon shadowing strength as exhibited in Fig. 1. MSTW08 with its zero gluon shadowing gives the largest rapidity distribution while EPS08, with its strong gluon shadowing, gives the smallest. Due to strong flux suppression, shadowing is most markedly apparent for the rapidity range $-2 \lesssim y \lesssim 2$. This range therefore provides a good window to discriminate among different gluon shadowing scenarios.

The rapidity interval $3 < y < 6$ corresponds to $x_{\min}$ in the antishadowing region (deep shadowing) for right (left) incident photons and vice versa for $-6 < y < -3$. Due to the photon flux suppression in the deep shadowing region, the rapidity distributions are sensitive mainly to antishadowing in addition to both EMC effect and Fermi motion. Since both EPS08 and EPS09 have substantial antishadowing, their rapidity distributions reflect this, being slightly larger than those from HKN07 and MSTW08. The discriminatory power here is not as appreciable as in the shadowing case, however, largely due to the smallness of the distributions.

For both rapidity ranges $y < -6$ and $y > 6$, $x_{\min} > 0.2$ and the relevant contributing nuclear effects are the EMC and Fermi motion since the contribution from antishadowing is small, and that from shadowing practically nonexistent by virtue of flux suppression. Due to the behavior of HKN07 in this interval (no EMC effect, only enhancement), $d\sigma/dy$ from HKN07 is largest. Both EPS08 and EPS09 nuclear modifications exhibit EMC effect and Fermi motion, and the destructive interference from both effects render their rapidity distributions to practically coincide with that from MSTW08.

In Table I we present the total cross section for the direct photoproduction of $c\bar{c}$ at two different scales, as discussed earlier. For both scales the cross sections exhibit a clear trend in conformity with the relative strength of gluon shadowing. MSTW08 with no modifications gives the largest cross section while EPS08 gives the smallest, due to its strong gluon shadowing. It is also noteworthy that the static scale gives lower cross sections relative to the dynamic scale. The difference between the two scales increases progressively with

TABLE I. Total cross sections for direct photoproduction of $c\bar{c}$ in ultraperipheral Pb-Pb collisions at the LHC. All cross sections are in millibarns (mb).

Gluon distribution	$Q^2 = \hat{s}$	$Q^2 = 4m_c^2$
MSTW08	1170	1090
EPS08	890	780
EPS09	1000	910
HKN07	1080	1000

TABLE II. Total cross sections for direct photoproduction of $b\bar{b}$ in ultraperipheral Pb-Pb collisions at the LHC. All cross sections are in millibarns (mb).

Gluon distribution	$Q^2 = \hat{s}$	$Q^2 = m_b^2$
MSTW08	6.2	7.0
EPS08	5.8	6.2
EPS09	6.0	6.6
HKN07	6.1	6.7

increasing shadowing, from ≈7% for MSTW08 to around 13% for EPS08. Overall, the total cross section also seems to be a good discriminator of different gluon shadowing scenarios.

Our cross sections can be compared with results from other studies on $c\bar{c}$ photoproduction. In [10,39] the cross section with no shadowing (equivalent to our MSTW08) is 1250 mb, from EKS98 [18] (somewhat akin to EPS09) it is 1050 mb, while from FGS (strong shadowing as in EPS08) [24] it is 850 mb. Likewise in [8] the no-shadowing cross section is 1790 mb while the cross section from EKS98 is 1500 mb. The study in [9] gives the cross section as 2056 mb. Overall, our results are closest to those reported in [10,39]. Differences in results are not only attributable to the different gluon distributions and photon fluxes used in the earlier studies, but also possibly to different values of the running strong coupling, $\alpha_s(Q^2)$, which enters multiplicatively in the expression for the photon-gluon cross section.

We now discuss our result for the total cross sections and rapidity distributions for $b\bar{b}$ production. The cross sections are orders of magnitude less than in $c\bar{c}$ production, and also correspondingly exhibit less sensitivity to nuclear modifications. In Fig. 6 we show the rapidity distribution for $b\bar{b}$ in ultraperipheral Pb-Pb collisions at the LHC. Shadowing dominates in the rapidity interval $-2 < y < 2$ and is most clearly manifested in the rapidity window $-1 < y < 1$. Thus

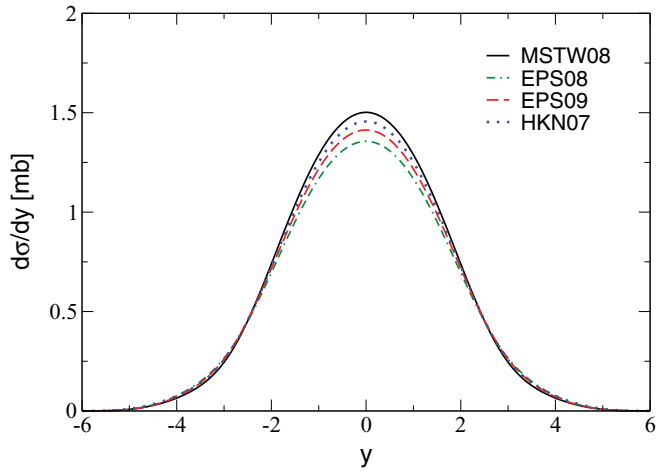

FIG. 6. (Color online) Total rapidity distributions of $b\bar{b}$ photoproduction in Pb-Pb collisions at the LHC. Solid line depicts the result using the MSTW08 gluon distribution (no nuclear modifications). Dashed, dot-dashed, and dotted lines are results from nuclear-modified gluon distributions from EPS09, EPS08, and HKN07 parton distributions, respectively.

this interval presents the best sensitivity to shadowing effects in $b\bar{b}$ production. Although less marked, the progression of rapidity distribution with relative shadowing strength follows the trend observed in $c\bar{c}$ production: MSTW08 still gives the largest distribution while EPS08 gives the smallest.

As in the case of $c\bar{c}$ production, there is a slight manifestation of the influence of antishadowing around $y = -3$ and $y = 3$. The distributions practically overlap for $y < -4$ and $y > 4$; thus overall, the interval $-1 \lesssim y \lesssim 1$ seems to afford the best sensitivity to nuclear effects, in this case primarily shadowing. More detailed treatment of the x dependence of $b\bar{b}$ production at the LHC is presented in [40].

The total photoproduction cross sections for $b\bar{b}$ from the four gluon distributions are presented in Table II. It is readily observed from the table that nuclear modifications have manifestly weaker effects on $b\bar{b}$ production relative to $c\bar{c}$, since the results from two widely different distributions like MSTW08 and EPS08 are almost in the same ballpark. This observation is also apparently scale independent. Unlike the $c\bar{c}$ case though, the static scale gives larger cross sections than the dynamic scale, and the difference decreases with relative shadowing strength.

Our cross sections can be compared with results from other studies on $b\bar{b}$ photoproduction. In [10,39] the cross section with no shadowing is 4.9 mb, from EKS98 it is 4.7 mb, while from FGS it is 4.4 mb. Likewise in [8] the no-shadowing cross section is 0.718 mb while the cross section from EKS98 is 0.686 mb. The study in [9] gives the cross section as 20.1 mb. Again, our results are closest to the values reported in [10]. The comment concerning the differences in the $c\bar{c}$ results is also applicable here. Additional details can be found in [9].

It is pertinent at this point to remark on the limitations inherent in our calculated cross sections for both $c\bar{c}$ and $b\bar{b}$ photoproduction. The results are to leading order; thus higher-order effects have not been taken into account either explicitly or through a phenomenological correction factor. In addition, we have not included the resolved contributions, which are quite sizable (see [8]). We thus advocate that these limitations should be borne in mind, more so in view of the disparities in cross-section results from the present work and previous studies.

VI. GLUON MODIFICATIONS IN ELASTIC PHOTOPRODUCTION OF VECTOR MESONS

We now present our results on elastic photoproduction of the J/Ψ and $\Upsilon(1s)$ in the framework of a leading-order

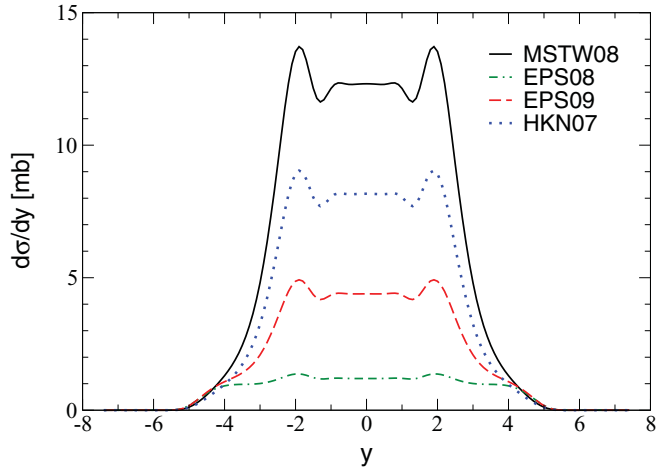

FIG. 7. (Color online) Total rapidity distributions of exclusive photoproduction of J/Ψ in Pb-Pb collisions at the LHC in the modified hard-sphere density distribution approximation. Solid line depicts the result using the MSTW08 gluon distribution (no nuclear modifications). Dashed, dot-dashed, and dotted lines are results from nuclear-modified gluon distributions from EPS09, EPS08, and HKN07 parton distributions, respectively.

two-gluon exchange formalism in QCD. Apart from the quadratic dependence on the gluon distribution, two other quantities, namely, the integrated nuclear form factor and the photon flux, affect the attributes of both the rapidity distribution and total cross section. The photon flux has support at low photon energy k, which translates to large x, while the integrated form factor favors large k, or equivalently, small x.

Figure 7 shows the rapidity distribution of the J/Ψ in ultraperipheral Pb-Pb collisions at the LHC. Shadowing is the relevant nuclear effect in the rapidity interval $-3 < y < 3$ and unsurprisingly, the rapidity distributions mimic the behavior in the shadowing region of Fig. 1. The largest rapidity distribution is given by MSTW08, followed by HKN07, and EPS09. The smallest is by EPS08 due to its strong gluon shadowing. The rapidity window $-2 < y < 2$ manifestly depicts the significant distinction between the various gluon distributions arising from the quadratic dependence. Antishadowing manifests in the intervals $-5 < y < -4$ and $4 < y < 5$; the effect, however, is quite slight.

Table III shows the total cross sections for the elastic photoproduction of the J/Ψ using the four gluon distributions considered in our study. The leading order result is shown in the second column while the corrected leading order result is shown in the third. As expected, the total cross sections reproduce the trend seen in the rapidity distributions: MSTW08 gives the largest cross section while EPS08 yields the smallest.

TABLE III. Total cross sections (in mb) for elastic photoproduction of J/Ψ in ultraperipheral Pb-Pb collisions at the LHC. Second column displays the results from LO calculation while the third column displays results from corrected LO calculation.

Gluon distribution	LO	Corrected LO
MSTW08	260	74
EPS08	36	10
EPS09	101	29
HKN07	173	49

TABLE IV. Total cross sections (in μb) for elastic photoproduction of J/Ψ in ultraperipheral Au-Au collisions at RHIC.

Gluon distribution	LO	Corrected LO
MSTW08	1222	349
EPS08	699	200
EPS09	868	248
HKN07	902	258

There have been studies of the photoproduction of J/Ψ in ultraperipheral collisions at LHC using diverse production mechanisms [5,7,11,12,41–44]. Here, since we are interested in the sensitivity to gluon modifications, we use the simple leading order two-gluon exchange mechanism corrected for additional relevant effects through a multiplicative factor. Our work is similar in spirit to the study reported in [12] in the sense that four different gluon distributions were also utilized. Thus we compare our results to the work in [12] which reports a no-shadowing cross section of 74 mb, a cross section from EPS08 of 13 mb, from EKS98 of 39 mb, and from DS03 [19] (somewhat similar to HKN07) of 61 mb. While the corrected LO results are somewhat close to these values, the uncorrected LO results presented in Table III are consistently higher.

In Table IV we also present the equivalent cross sections for J/Ψ production in ultraperipheral Au-Au collisions at the Relativistic Heavy Ion Collider. As is readily apparent, the results follow the shadowing trend as observed for Pb-Pb collisions at the LHC.

The rapidity distributions for $\Upsilon(1s)$ production are shown in Fig. 8, and exhibit the identical trend observed for J/Ψ.

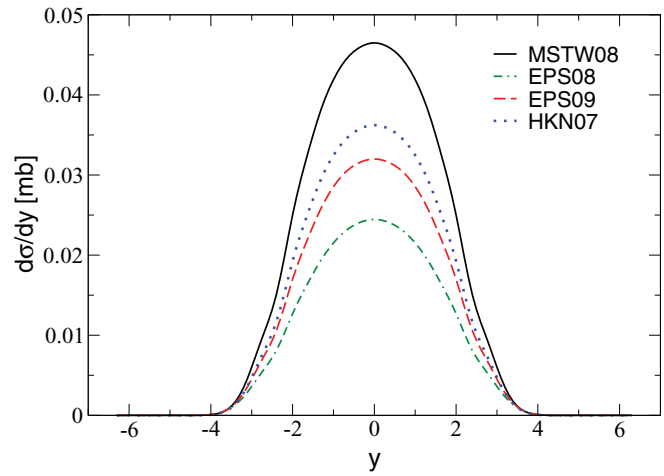

FIG. 8. (Color online) Total rapidity distributions of exclusive photoproduction of $\Upsilon(1s)$ in Pb-Pb collisions at the LHC in the modified hard-sphere density distribution approximation. Solid line depicts the result using the MSTW08 gluon distribution (no nuclear modifications). Dashed, dot-dashed, and dotted lines are results from nuclear-modified gluon distributions from EPS09, EPS08, and HKN07 parton distributions, respectively.

TABLE V. Total cross sections for elastic photoproduction of $\Upsilon(1s)$ in ultraperipheral Pb-Pb collisions at the LHC.

Gluon distribution	Cross section (μb)
MSTW08	189
EPS08	99
EPS09	130
HKN07	146

Shadowing remains the relevant nuclear modification for practically the entire rapidity range shown in the figure, and is markedly manifested in the interval $-2 < y < 2$. Thus rapidity distribution in this interval should be a good discriminator of gluon shadowing strength.

In Table V we show the total cross sections for the elastic photoproduction of the $\Upsilon(1s)$ for the four gluon distributions under study. Unsurprisingly, the total cross sections reflect the progressive trend of the relative shadowing strength, with MSTW08 giving the largest cross section while EPS08 yields the smallest.

Previous studies of the photoproduction of $\Upsilon(1s)$ in ultraperipheral collisions at LHC energies have been reported in [12,38,43,45]. As in the case of J/Ψ production, we compare our results with the values reported in [12]. The no-shadowing cross section is 163 μb, from EPS08 22 μb, from EKS98 120 μb, and from DS03 148 μb. Except for the case of EPS08, our results presented in Table V are quite close to these values.

VII. CONCLUSIONS

In conclusion, we have considered the direct photoproduction of heavy quarks (charm and bottom) and elastic photoproduction of vector mesons [J/Ψ and $\Upsilon(1s)$] in ultraperipheral Pb-Pb collisions at LHC energy. These two processes are dependent on nuclear gluon distributions, and are therefore potentially useful in constraining modifications such as shadowing and antishadowing in nuclear gluon distributions. In order to assess the sensitivity to these modifications, we have utilized four recent gluon distributions chosen on the basis of the relative strength of their modifications. For each process we considered two observables: rapidity distributions and total cross sections.

In direct photoproduction of heavy quarks the gluon dependence is linear, and different modifications are superimposed due to the integration over the momentum fraction x. Despite these, rapidity distributions for $c\bar{c}$ manifest appreciable sensitivity to shadowing around midrapidity and a slight sensitivity to antishadowing at more forward and backward rapidities. Thus $c\bar{c}$ photoproduction offers good constraining potential for shadowing, and a somewhat less potential for antishadowing. Although photoproduction of $b\bar{b}$ is less sensitive to modifications than $c\bar{c}$, the influence of shadowing is evident around midrapidity, and it thus offers some constraining ability for shadowing.

The quadratic dependence on gluon modifications makes elastic photoproduction of vector mesons particularly attractive for constraining purposes. This is manifestly apparent from the rapidity distributions for both J/Ψ and $\Upsilon(1s)$ photoproduction, which exhibit very good sensitivity to gluon shadowing over an appreciable range about midrapidity. Thus both offer remarkable potential in constraining the shadowing component of nuclear gluon distributions.

Determination of nuclear modifications from *ab initio* calculations of cross sections is beset with difficulties. A more feasible approach is to compare photoproduction in proton-nucleus and nucleus-nucleus collisions, where many theoretical uncertainties and systematic errors cancel (see [46]). Further work along this line is in progress.

ACKNOWLEDGMENTS

We acknowledge support by the US Department of Energy Grant Nos. DE-FG02-08ER41533 and DE-FC02-07ER41457 (UNEDF, SciDAC-2) and the Research Corporation.

[1] E. Fermi, Z. Phys. **29**, 315 (1924); Nuovo Cimento **2**, 143 (1925).
[2] C. A. Bertulani and G. Baur, Phys. Rep. **163**, 299 (1988).
[3] R. N. Cahn and J. D. Jackson, Phys. Rev. D **42**, 3690 (1990).
[4] G. Baur and L. G. Ferreira Filho, Nucl. Phys. A **518**, 786 (1990).
[5] S. R. Klein and J. Nystrand, Phys. Rev. C **60**, 014903 (1999).
[6] C. A. Bertulani and D. S. Dolci, Nucl. Phys. A **674**, 527 (2000).
[7] V. P. Goncalves and C. A. Bertulani, Phys. Rev. C **65**, 054905 (2002).
[8] S. R. Klein, J. Nystrand, and R. Vogt, Phys. Rev. C **66**, 044906 (2002).
[9] V. P. Goncalves and M. V. T. Machado, Eur. Phys. J. C **31**, 371 (2003).
[10] C. A. Bertulani, S. R. Klein, and J. Nystrand, Annu. Rev. Nucl. Part. Sci. **55**, 271 (2005).
[11] A. J. Baltz *et al.*, Phys. Rep. **458**, 1 (2008).
[12] A. L. Ayala Filho, V. P. Goncalves, and M. T. Griep, Phys. Rev. C **78**, 044904 (2008).
[13] J. J. Aubert *et al.* (European Muon Collaboration), Phys. Lett. B **123**, 275 (1983).
[14] D. F. Geesaman, K. Saito, and A. W. Thomas, Annu. Rev. Nucl. Part. Sci. **45**, 337 (1995).
[15] G. Piller and W. Weise, Phys. Rep. **330**, 1 (2000).
[16] N. Armesto, J. Phys. G **32**, R367 (2006).
[17] V. J. Kolhinen, arXiv:hep-ph/0506287.
[18] K. J. Eskola, V. J. Kolhinen, and C. A. Salgado, Eur. Phys. J. C **9**, 61 (1999).
[19] D. de Florian and R. Sassot, Phys. Rev. D **69**, 074028 (2004).
[20] M. Hirai, S. Kumano, and T. H. Nagai, Phys. Rev. C **70**, 044905 (2004); Nucl. Phys. Proc. Suppl. **139**, 21 (2005).
[21] M. Hirai, S. Kumano, and T. H. Nagai, Phys. Rev. C **76**, 065207 (2007).
[22] K. J. Eskola, H. Paukkunen, and C. A. Salgado, J. High Energy Phys. 07 (2008) 102.

[23] K. J. Eskola, H. Paukkunen, and C. A. Salgado, J. High Energy Phys. 04 (2009) 065.
[24] L. Frankfurt, V. Guzey, and M. Strikman, Phys. Rev. D **71**, 054001 (2005).
[25] A. D. Martin, W. J. Stirling, R. S. Thorne, and G. Watt, Eur. Phys. J. C **63**, 189 (2009).
[26] M. Gluck and E. Reya, Phys. Lett. B **79**, 453 (1978).
[27] L. M. Jones and H. W. Wyld, Phys. Rev. D **17**, 759 (1978).
[28] H. Fritzsch and K. H. Streng, Phys. Lett. B **72**, 385 (1978).
[29] M. G. Ryskin, Z. Phys. C **57**, 89 (1993).
[30] S. J. Brodsky, L. Frankfurt, J. F. Gunion, A. H. Mueller, and M. Strikman, Phys. Rev. D **50**, 3134 (1994).
[31] M. G. Ryskin, R. G. Roberts, A. D. Martin, and E. M. Levin, Z. Phys. C **76**, 231 (1997).
[32] L. Frankfurt, W. Koepf, and M. Strikman, Phys. Rev. D **57**, 512 (1998).
[33] C. Adloff *et al*. (H1 Collaboration), Phys. Lett. B **483**, 23 (2000).
[34] J. Breitweg *et al*. (ZEUS Collaboration), Phys. Lett. B **437**, 432 (1998).
[35] S. Chekanov *et al*. (ZEUS Collaboration), Phys. Lett. B **680**, 4 (2009).
[36] C. W. De Jager, H. De Vries, and C. De Vries, At. Data Nucl. Data Tables **14**, 479 (1974).
[37] K. T. R. Davies and J. R. Nix, Phys. Rev. C **14**, 1977 (1976).
[38] S. R. Klein and J. Nystrand, Phys. Rev. Lett. **92**, 142003 (2004).
[39] R. Vogt (private communication).
[40] M. Strikman, R. Vogt, and S. N. White, Phys. Rev. Lett. **96**, 082001 (2006).
[41] L. Frankfurt, M. Strikman, and M. Zhalov, Phys. Lett. B **540**, 220 (2002).
[42] V. P. Goncalves and M. V. T. Machado, Eur. Phys. J. C **40**, 519 (2005).
[43] V. P. Goncalves and M. V. T. Machado, Phys. Rev. D **77**, 014037 (2008).
[44] Yu. P. Ivanov, B. Z. Kopeliovich, and I. Schmidt, arXiv:0706.1532 [hep-ph].
[45] L. Frankfurt, V. Guzey, M. Strikman, and M. Zhalov, J. High Energy Phys. 08 (2003) 043.
[46] C. A. Salgado *et al*., arXiv:1105.3919 [hep-ph].